

Incipient Orbital Order in Half-Metallic $\text{Ba}_2\text{FeReO}_6$

C. Azimonte,^{1,2} J. C. Cezar,³ E. Granado,^{1,2,*} Q. Huang,⁴ J. W. Lynn,^{4,5} J. C. P. Campoy,¹
J. Gopalakrishnan,^{5,6} and K. Ramesha⁶

¹*Instituto de Física “Gleb Wataghin,” UNICAMP, C.P. 6165, 13083-970, Campinas, São Paulo, Brazil*

²*Laboratório Nacional de Luz Síncrotron, C.P. 6192, 13084-971, Campinas, São Paulo, Brazil*

³*European Synchrotron Radiation Facility, F-38043, Grenoble, France*

⁴*NIST Center for Neutron Research, National Institute of Standards and Technology, Gaithersburg, Maryland 20899, USA*

⁵*Center for Superconductivity Research, University of Maryland, College Park, Maryland 20742, USA*

⁶*Solid State and Structural Chemistry Unit, Indian Institute of Science, Bangalore 560012, India*

(Received 16 May 2006; published 5 January 2007)

Largely unquenched Re 5*d* orbital magnetic moments in half-metallic $\text{Ba}_2\text{FeReO}_6$ drive a symmetry lowering transition from a cubic paramagnet to a compressed tetragonal ($c/a < 1$) ferrimagnet below $T_C \sim 305$ K, with a giant linear magnetoelastic constant and the spins lying spontaneously along the unique tetragonal axis. The large orbital magnetization and degree of structural deformation indicate proximity to a metal-insulator transition. These results point to an incipient orbitally ordered state in the metallic ferrimagnetic phase.

DOI: [10.1103/PhysRevLett.98.017204](https://doi.org/10.1103/PhysRevLett.98.017204)

PACS numbers: 75.50.Gg, 61.10.Nz, 61.12.Ld, 71.30.+h

The overwhelming majority of studies on orbital ordering and its relationship with magnetism and crystal structures has been done in 3*d* or 4*d* oxide systems such as manganites, vanadates, and ruthenates [1]. 5*d* elements, on the other hand, are generally nonmagnetic and orbitally inactive in the solid state, being nonetheless at the verge of magnetism. For this reason, hybridization of 5*d* electrons with 3*d* magnetic electrons of nearby ions [2], or even particle size effects [3] may trigger the 5*d* magnetism. A particularly interesting case is the $A_2\text{FeReO}_6$ ($A = \text{Ca}, \text{Sr}, \text{Ba}$) double perovskites. This structure is characterized by a three-dimensional network of alternating FeO_6 and ReO_6 octahedra, with the A^{2+} ions being charge donors outside the octahedra. The Re moments are found to define a periodic ferromagnetic sublattice that is antiferromagnetically coupled to the Fe 3*d* moments. The system is half-metallic for $A = \text{Sr}$ and Ba and the spin-polarized conduction electrons show primarily Re 5*d* character, while showing semiconducting transport behavior for $A = \text{Ca}$ [4–11]. In addition, this family has been attracting increasing interest due to the potential use in spintronics devices. A marked feature of this particular system is the presence of large magnetic anisotropy effects associated with unquenched Re 5*d* orbital magnetic moments due to strong spin-orbit coupling [8–14]. Here, we investigate in detail the crystal structure and local magnetism of $\text{Ba}_2\text{FeReO}_6$ (BFRO) by means of *T*- and *H*-dependent high-resolution synchrotron x-ray powder diffraction (SXPd), neutron powder diffraction (NPD), and Re and Fe $L_{2,3}$ -edges x-ray magnetic circular dichroism (XMCD) experiments. Our results indicate an incipient orbital-ordering transition of Re 5*d* orbitals in the metallic phase. This appears to be characteristic of the 5*d* magnetism [13], since the orbital degree of freedom tends to be much less pronounced, or completely quenched, in the metallic state of 3*d* or 4*d* systems.

Polycrystalline BFRO was grown by solid state reaction [7,15], with a minor Fe_3O_4 impurity phase [2.1(1)% weight fraction] detected by x-ray and neutron diffraction measurements. Resistivity characterization confirmed a metallic behavior between 20 and 350 K [7], with a low-*T* intergrain magnetoresistance of $\sim 5\%$ at 1 T [15], increasing at larger fields. NPD measurements were taken on the BT-1 diffractometer at the NIST Center for Neutron Research, using monochromatic beams with 1.5402(1) Å and 2.0783(1) Å [16]. SXPd data were collected under reflection geometry on the x-ray powder diffraction (XPd) beam line at the Laboratório Nacional de Luz Síncrotron (LNLS) [17], using an incident beam with $\lambda = 1.3773$ Å and a Ge(111) analyzer crystal. XMCD measurements at the Re $L_{2,3}$ -edges were performed on the dispersive x-ray absorption beam line at LNLS [18], with a calculated degree of circular polarization of $\sim 77\%$. The energy resolutions at the L_3 (10.53 keV) and L_2 (11.96 keV) edges are 2.7 and 3.4 eV, respectively. The Re $L_3:L_2$ edge jump ratio in the x-ray absorption (XAS) spectra was normalized to 2.17, following Ref. [19]. A rotative permanent magnet applied 0.9 T at the sample, both parallel and antiparallel to the x-ray beam direction. The same magnet was used to perform field-dependent SXPd experiments, which were taken on a pelletized sample to avoid any physical rotation of the grains with the field. The XMCD signal at the Fe $L_{2,3}$ -edges was measured at the European Synchrotron Radiation Facility, beam line ID08. The pelletized sample was scraped *in situ* and maintained at 5×10^{-10} mbar. The spectra were measured in total electron yield mode, changing both the direction of the 5.5 T applied magnetic field and the ellipticity of the fully circular polarized x-ray beam.

Figures 1(a) and 1(b) show selected portions of the NPD and SXPd profiles of BFRO at 14 K. A deviation from the

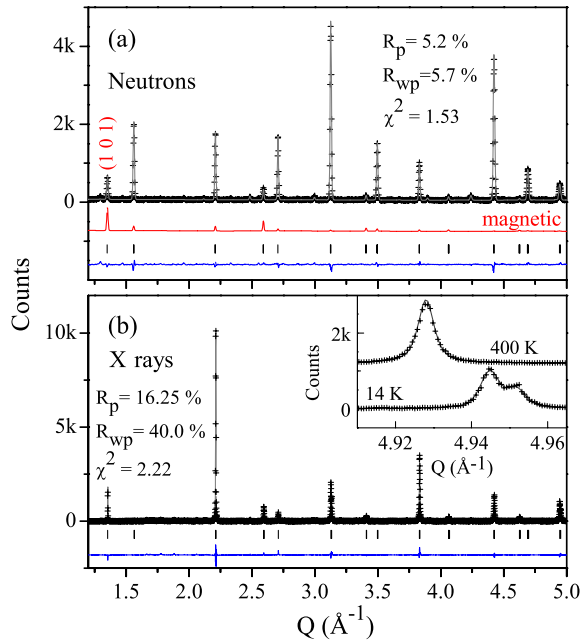


FIG. 1 (color online). (a) Neutron and (b) synchrotron x-ray powder diffraction (SXP) profiles at 14 K. The cross symbols and gray solid lines show the experimental data and calculated intensities according to the $I4/mmm$ structural model (see text), respectively. The difference profiles are also given as solid lines. The short vertical bars indicate the Bragg positions. The calculated magnetic contributions to the neutron data according to a simple ferrimagnetic model of Fe and Re spins (see text) are given in (a) as a solid red (dark gray) line below the experimental profile. The inset in (b) shows in detail a selected portion of SXP data at 14 and 400 K. Error factors for the whole-profile Rietveld refinements are given.

cubic double perovskite structure is clearly observed at this temperature [see inset of Fig. 1(b)]. Combined crystal and magnetic structure refinements using both SXP and NPD data were carried out using the program GSAS [20]. Preliminary refinements were performed assuming three distinct structural models: (i) a tetragonal model with $I4/mmm$ symmetry [21], allowing for distortions of the FeO_6 and ReO_6 octahedra; (ii) a tetragonal model with $I4/m$ symmetry allowing for octahedral distortions as well as rotations along the (001) axis [22]; and (iii) a monoclinic model with $P2_1/n$ symmetry, allowing for distortions and rotations of the octahedra along the (110) and (001) axes (cubic notation) [16]. Stable refinements and excellent fits to both NPD and SXP data were obtained with model (i), while no additional improvement was obtained for models (ii) and (iii). We conclude that the tetragonal symmetry is associated to the distortions of oxygen octahedra allowed by the $I4/mmm$ symmetry. Results of the combined refinement at 14 K and room- T are given in Ref. [23]. Bond-valence calculations [24] using the refined Fe–O bond distance at room- T [23] yield an Fe valence of +2.45.

Figure 2(a) shows the relative tetragonal distortion, $(a - c/\sqrt{2})/a$ (solid circles), obtained from the Rietveld refine-

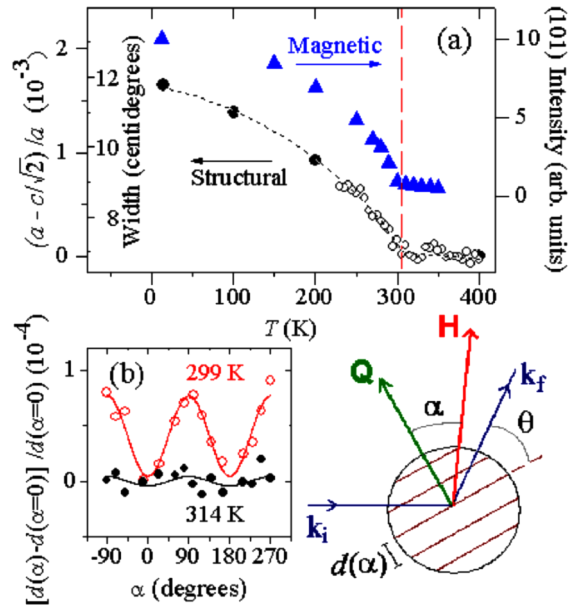


FIG. 2 (color online). (a) A comparison between zero-field magnetic and structural order parameters. The first is represented by the (101) neutron Bragg reflection [see Fig. 1(a)]. The structural counterpart was directly obtained from the tetragonal deformation $(a - c/\sqrt{2})/a$ (solid circles) taken from the Rietveld refinements and by the 2θ full width at half maximum of the (220)/(004) Bragg reflections in the synchrotron x-ray data, which merge into a single peak above ~ 200 K (open circles), within our resolution. (b) Relative variation of the average Bragg interplanar distance d of the (220)/(004) reflections as a function of the angle α between an applied magnetic field of $H = 0.9$ T and the direction of the momentum transfer Q , at 299 K ($< T_c$) and 314 K ($> T_c$).

ments below 200 K. It decreases on warming, following a typical critical behavior. The Bragg peaks that are clearly split in the synchrotron data at lower T merge into a single broadened peak above 200 K, within our resolution. The tetragonal deformation above 200 K was then indirectly probed by the (004)/(220) peak width (open circles), which decreases on warming up to $T_s = 309(5)$ K, marking the transition from the tetragonal to the cubic double perovskite phase. In fact, refinements performed under $Fm3m$ space group yield highly satisfactory results above T_s .

An analysis of the NPD profiles at low- T show the presence of magnetic contributions [see Fig. 1(a)], which could be well accounted for in the refinements by a simple ferrimagnetic model of Fe and Re moments. Theoretical magnetic form factors for Fe^{3+} (Ir^{4+}) were used for the Fe (Re) $3d$ ($5d$) moments [25,26]. The relatively small (Fe,Re)-site disorder in this sample [4(1)%] was taken into account by assuming that mis-site Fe spins are antiferromagnetically coupled to the main Fe sublattice, with a similar assumption for the mis-site Re spins. Under the above procedure, the refined moments are $\mu(\text{Fe}) = 3.16(10)\mu_B$ and $\mu(\text{Re}) = -1.08(13)\mu_B$ at 14 K. Figure 2(a) shows the T dependence of the neutron inten-

sity of the (101) magnetic reflection, which is proportional to $[\mu(\text{Fe}) - \mu(\text{Re})]^2$. The magnetic ordering transition is seen to take place at $T_C = 304(3)$ K.

To show that the coincidence of the magnetic and structural transitions is not accidental as in $\text{Sr}_2\text{FeMoO}_6$ [22], the average Bragg d spacing for the (004)/(220) overlapped peak was measured as a function of the angle between the scattering vector Q and an applied magnetic field $H = 0.9$ T, at T slightly below and above the transitions [see Fig. 2(b)]. Below T_C , a clear magnetostructural coupling is observed, which vanishes in the paramagnetic phase. The minimum d is measured for $H \parallel Q$, while the maximum d is observed for $H \perp Q$. This demonstrates that the crystal structure is compressed along the magnetic moment direction. Since $c/a < 1$, the spins are oriented along the tetragonal c axis below T_C in the absence of an external field. The above results unambiguously show the magnetoelastic nature of the tetragonal transition. The linear magnetoelastic constant at 10 K can be extracted from the relation $\lambda_{100} = \frac{2}{3}[(a - c/\sqrt{2})/a] = 1.1 \times 10^{-3}$, which is a giant value for metallic transition-metal systems [27]. A magnetostriction effect of similar magnitude has been recently observed for $\text{Ca}_2\text{FeReO}_6$ [14], and a compression of the lattice along the magnetic moment direction was observed in the insulating phase of this compound [13,16].

Insight into the large linear magnetoelastic coupling is gained by an x-ray spectroscopic investigation of the nature of the Fe and Re magnetic moments. Figures 3(a) and 3(c) display the XAS spectra at the Re $L_{2,3}$ -edges and Fe $L_{2,3}$ -edges, respectively, at $T = 10$ K, while Figs. 3(b) and 3(d) show the corresponding XMCD spectra in the energy

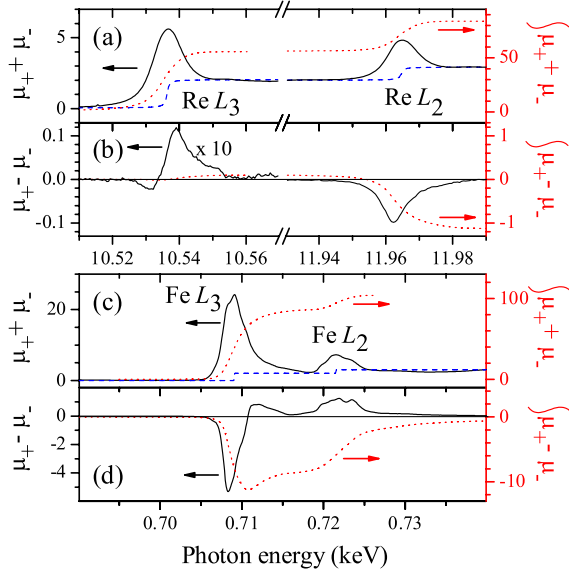


FIG. 3 (color online). X-ray absorption (XAS, $\mu_+ + \mu_-$) and x-ray magnetic circular dichroism (XMCD, $\mu_+ - \mu_-$) spectra at the Re $L_{2,3}$ (a),(b) and Fe $L_{2,3}$ (c),(d) absorption edges (solid lines). The edge jumps are given in (a) and (c) as blue (dark gray) dashed lines. The dotted lines in red (gray) in (a)–(d) indicate the XAS and XMCD integration.

intervals where significant contributions to the XMCD integral have been observed. Well known sum rules relate the integrated XAS and XMCD signals [dotted lines in Figs. 3(a)–3(d)] to the orbital, spin, and dipole magnetic moments [28]. For polycrystalline samples, the expectation value of the dipole operator may be neglected [29], and both the spin and orbital moments may be directly extracted from the XMCD spectra. Nonetheless, a correction to the spin sum rule must be used for the Fe spin moments, associated with the relatively weak spin-orbit coupling in the Fe $2p$ core holes [30]. In the present case, we use a correction term $2/(0.875 + 0.685)$ for the Fe spin moments extracted from the sum rules, which is an average of the calculated corrections for Fe^{2+} and Fe^{3+} [30]. In addition, corrections for the degree of circular polarization, nonsaturation of magnetic domains at the fields used in the XMCD experiments (estimated from $M \times H$ bulk measurements), and (Fe, Re) site disorder are included in the calculations. Finally, it is necessary to include the Fe $3d$ and Re $5d$ electron occupation numbers in the calculations (n_{3d} and n_{5d} , respectively) [28]. Here, we use $n_{5d} = 4.5$ and $n_{3d} = 5.93$ calculated based on the local spin density approximation with on-site Coulomb correlation correction (LSDA + U) [5]. Under the above procedure, we obtain for the Re moments $\mu_{\text{orb}}/\mu_{\text{spin}}(\text{Re}) = -0.294(3)$, $\mu_{\text{orb}}(\text{Re}) = 0.19(1)\mu_B$, $\mu_{\text{spin}}(\text{Re}) = -0.64(4)\mu_B$, and thus $\mu_{\text{total}}(\text{Re}) = -0.45(5)\mu_B$; for the Fe moments, the following values were obtained: $\mu_{\text{orb}}/\mu_{\text{spin}}(\text{Fe}) = 0.013(7)$, $\mu_{\text{orb}}(\text{Fe}) = 0.04(2)\mu_B$, and $\mu_{\text{spin}}(\text{Fe}) = 2.8(2)\mu_B$. The negative (positive) sign of $\mu_{\text{orb}}/\mu_{\text{spin}}$ for Re (Fe) ions agree with the predictions of the third Hund's rule for less (more) than half-filled d shell for $\text{Re}^{5.55+}$ ($\text{Fe}^{2.45+}$) ions, and its large value for Re is consistent with Ref. [12] and comparable to theoretical predictions for $\text{Sr}_2\text{FeReO}_6$ [8]. Also, the Fe total moment extracted from XMCD agrees well with the neutron value (see above), while the Re total moment is significantly smaller. The spin moments in both ions are smaller by ~ 25 – 50% than predicted by LSDA and LSDA + U calculations for this compound [5]. Further work is necessary to account for the origin of such discrepancies.

Perhaps the most interesting observations from XMCD experiments are the largely unquenched (quenched) Re (Fe) orbital moments. The ratio $\mu_{\text{orb}}/\mu_{\text{spin}}(\text{Re}) \sim -0.3$ may be compared with the ideal atomistic values $\mu_{\text{orb}}/\mu_{\text{spin}}(\text{Re}^{5+}) = -0.5$ with complete occupation of $(yz - izx)$ and (xy) orbitals and empty $(yz + izx)$, or $\mu_{\text{orb}}/\mu_{\text{spin}}(\text{Re}^{6+}) = -1$ with complete occupation of $(yz - izx)$ orbital and empty (xy) and $(yz + izx)$ levels. This comparison shows that the Re $5d$ conduction electrons present a high degree of orbital polarization in the metallic state. In fact, a relevant spin-orbit coupling would reduce the energy of the $(yz - izx)$ level with unquenched orbital moment, with respect to the (xy) and $(yz + izx)$ orbitals. In metallic systems with partly occupied t_{2g} bands, that may lead to a large unquenched orbital moment

only if the spin-orbit energy is comparable to the conduction bandwidth (~ 1 eV). Although this is never the case for $3d:t_{2g}$ metallic systems, the spin-orbit coupling in $5d$ ions [8] may be of the order of the conduction bandwidth. For example, in atomic physics the spin-orbit splittings between the $3P_0$ and $3P_2$ terms in elemental Hf ($5d^2$) and Ti ($3d^2$), are 0.43 and 0.02 eV, respectively [31].

In conclusion, a large Re $5d$ spin-orbit coupling [8–12], possibly allied to significant in-site Coulomb correlation effects [16,32], is responsible for a large orbital polarization of the conduction electrons in half-metallic $\text{Ba}_2\text{FeReO}_6$. This experimental (see above) and theoretical [8] fact, as well as the observation of a semiconductor behavior in isoelectronic $\text{Ca}_2\text{FeReO}_6$, indicate that the conduction electrons in the title compound are in the proximity of a metal-insulator transition. This is likely related to the giant magnetoelastic coupling observed here. We emphasize that this structural effect has the same physical origin as the normal magnetostriction effect observed in most metallic transition-metal systems, namely, the anisotropy of the charge density distribution of the occupied d states. However, in the present case the magnitude of the effect is amplified by the unusually large orbital polarization revealed by XMCD data, resulting in a lattice distortion that is about 2 orders of magnitude larger than typical reported values for metallic transition-metal alloys and oxides [27]. Still, the lattice distortion remains about 1 order of magnitude smaller than normally found in insulating $3d:t_{2g}$ systems due to orbital ordering [33]. Thus, our results in $\text{Ba}_2\text{FeReO}_6$ provide a link between the large orbital-ordering effects commonly found in insulators with degenerate d orbitals and the much weaker conventional magnetostriction found in metallic transition-metal systems.

This work was supported by FAPESP, CNPq, FINEP, and ABTLuS, Brazil, and DST, New Delhi, India.

*Electronic address: egranado@ifi.unicamp.br

- [1] For a review, see Y. Tokura and N. Nagaosa, *Science* **288**, 462 (2000).
- [2] G. Schütz *et al.*, *Z. Phys. B* **75**, 495 (1989).
- [3] Y. Yamamoto *et al.*, *Phys. Rev. Lett.* **93**, 116801 (2004).
- [4] K.-I. Kobayashi *et al.*, *Phys. Rev. B* **59**, 11 159 (1999).
- [5] H. Wu, *Phys. Rev. B* **64**, 125126 (2001).
- [6] H. Kato *et al.*, *Phys. Rev. B* **65**, 144404 (2002).
- [7] W. Prellier *et al.*, *J. Phys. Condens. Matter* **12**, 965 (2000).
- [8] H.-T. Jeng and G. Y. Guo, *Phys. Rev. B* **67**, 094438 (2003).
- [9] T. Alamelu *et al.*, *J. Appl. Phys.* **91**, 8909 (2002).
- [10] J.M. De Teresa *et al.*, *J. Magn. Magn. Mater.* **290–291**, 1043 (2005).
- [11] J.M. De Teresa, D. Serrate, J. Blasco, M.R. Ibarra, and L. Morellon, *Phys. Rev. B* **69**, 144401 (2004).
- [12] M. Sikora *et al.*, condmat/0503358 (unpublished).
- [13] K. Oikawa *et al.*, *J. Phys. Soc. Jpn.* **72**, 1411 (2003).
- [14] D. Serrate *et al.*, *J. Magn. Magn. Mater.* **290–291**, 843 (2005).
- [15] J. Gopalakrishnan *et al.*, *Phys. Rev. B* **62**, 9538 (2000).
- [16] E. Granado *et al.*, *Phys. Rev. B* **66**, 064409 (2002).
- [17] F.F. Ferreira *et al.*, *J. Synchrotron Radiat.* **13**, 46 (2006).
- [18] H.C.N. Tolentino *et al.*, *Phys. Scr. T* **115**, 977 (2005).
- [19] B.L. Henke, E.M. Gullikson, and J.C. Davis, *At. Data Nucl. Data Tables* **54**, 181 (1993); see also www-cxro.lbl.gov.
- [20] C. Larson and R.B. Von Dreele, Los Alamos National Laboratory Report No. LAUR086-748, 1990 (unpublished).
- [21] S.B. Kim, B.W. Lee, and C.S. Kim, *J. Magn. Magn. Mater.* **242**, 747 (2002).
- [22] C. Ritter *et al.*, *Solid State Sci.* **6**, 419 (2004).
- [23] For the combined refinement at 14 K under the $I4/mmm$ space group, the refined lattice parameters are $a = 5.68265(6)$ Å and $c = 8.02334(14)$ Å, and the atomic positions and thermal factors are Ba(1/2, 0, 1/4), $B_{\text{iso}} = 0.68(3)$ Å²; Fe(0, 0, 0) and Re(0, 0, 1/2), $B_{\text{iso}} = 0.30(2)$ Å²; O_{basal}(0.256(2), 0.256(2), 0), $B_{\text{iso}} = 0.84(6)$ Å²; O_{apical}(0, 0, 0.260(2)), $B_{\text{iso}} = 0.1(1)$ Å². The relevant bond distances are: Re-O_{basal} = 1.96(2) Å, Re-O_{apical} = 1.92(2) Å, Fe-O_{basal} = 2.06(2) Å, and Fe-O_{apical} = 2.09(2) Å. At room temperature, the remaining tetragonal distortion is too small to be observed by the medium resolution neutron data, and the structure was refined under a cubic structure (space group $Fm\bar{3}m$) using only neutron data. The refined lattice parameter is $a = 8.05429(8)$ Å, and the atomic positions and thermal factors are: Ba(1/4, 1/4, 1/4), $B_{\text{iso}} = 0.57(2)$ Å²; Fe(1/2, 0, 0) and Re(0, 0, 0), $B_{\text{iso}} = 0.32(3)$ Å²; O(0.2422(1), 0, 0), $B_{11} = 0.45(3)$ Å², $B_{22} = B_{33} = 0.61(2)$ Å². The relevant bond distances at room- T are Re-O = 1.950(1) Å and Fe-O = 2.077(1) Å.
- [24] I.D. Brown, *Acta Crystallogr. Sect. B* **48**, 553 (1992).
- [25] P.J. Brown, in *International Tables for Crystallography*, edited by A.J.C. Wilson (Kluwer Academic Publishers, Dordrecht/Boston/London, 1995), Vol. C, pp. 391–399.
- [26] D.T. Cromer and J.T. Waber, LASL Report No. LA-3056, 1964 (unpublished); J.W. Lynn, G. Shirane, and M. Blume, *Phys. Rev. Lett.* **37**, 154 (1976).
- [27] R.M. Bozorth, *Ferromagnetism* (IEEE Press, New York, 1951), Chapt. 13; X.W. Li, A. Gupta, and G. Xiao, *Appl. Phys. Lett.* **75**, 713 (1999).
- [28] B.T. Thole, P. Carra, F. Sette, and G. van der Laan, *Phys. Rev. Lett.* **68**, 1943 (1992); P. Carra, B.T. Thole, M. Altarelli, and X. Wang, *Phys. Rev. Lett.* **70**, 694 (1993); C.T. Chen *et al.*, *Phys. Rev. Lett.* **75**, 152 (1995).
- [29] J. Stöhr and H. König, *Phys. Rev. Lett.* **75**, 3748 (1995).
- [30] Y. Teramura, A. Tanaka, and T. Jo, *J. Phys. Soc. Jpn.* **65**, 1053 (1996).
- [31] W.F. Meggers and C.E. Moore, *Natl. Bur. Stand. (U.S.), Monogr.* **153** (1976); P. Forsberg, *Phys. Scr.* **44**, 446 (1991); See also <http://physics.nist.gov/PhysRefData/Handbook>
- [32] H. Iwasawa *et al.*, *Phys. Rev. B* **71**, 075106 (2005).
- [33] P. Bordet *et al.*, *J. Solid State Chem.* **106**, 253 (1993).